Chemical Science

ROYAL SOCIETY OF CHEMISTRY

EDGE ARTICLE

View Article Online
View Journal

Cite this: DOI: 10.1039/d5sc04694g

All publication charges for this article have been paid for by the Royal Society of Chemistry

Received 26th June 2025
Accepted 10th September 2025

DOI: 10.1039/d5sc04694g

rsc.li/chemical-science

Making non-emissive [6]cycloparaphenylene fluorescent by simple multiple methyl substitution

Tomoki Kato,[a] Daiki Imoto,[a] Akiko Yagi*[ab] and Kenichiro Itami *[bcd]

We report the unexpected discovery that non-emissive [6]cycloparaphenylene ([6]CPP) can be made fluorescent by multiple additions of simple methyl groups. Dodecamethyl[6]CPP (Me_{12}[6]CPP) was synthesized using a gold-based macrocyclization method and isolated as a pair of isomers (rotamers), both of which fluoresce at 510–540 nm. Experimental and theoretical investigations revealed that multiple methyl substitutions suppress rotation around the phenylene units, enabling the individual rotamers to be isolated and their interconversion to be studied. This simple yet significant "methyl effect" in CPPs not only enhances our basic understanding of stereoelectronic effects in CPPs, but should also facilitate the design and application of CPP-based materials in various fields.

Since their first syntheses in the late 2000s,[1–5] cycloparaphenylenes (CPPs), simple carbon nanorings composed solely of *para*-connected benzene rings, have attracted significant interest in various fields such as materials science,[6,7] chemical biology,[8] and beyond.[9] CPPs have become iconic molecules in the emerging fields of molecular nanocarbon science.[10] CPPs promise unique physical properties due to their highly distorted structure and π-conjugated system. With the establishment of CPP synthesis methods,[1–5] many derivatizations and application-oriented functionalizations have been developed, leading to the synthesis of an extensive array of CPP derivatives.[6] Recently, CPP derivatives, in which substituents are introduced to all the phenylene units, have received particular interest because such multiple substitutions can change the properties significantly (Fig. 1A). CPPs substituted with phenyl,[11,12] methoxy,[13,14] silyl,[15] and halogen groups[16] have been reported. As demonstrated by S_NAr reactions of fluorinated CPPs (Fig. 1B), such all-phenylene-substituted CPPs are promising precursors for the synthesis of new carbon nanorings and carbon nanobelts *via* the transformation of reactive substituents (Fig. 1B).[16,17]

Although various CPP derivatives have been synthesized to date, CPPs with a simple methyl group have not been studied. This is understandable because the methyl group has a minimal stereoelectronic effect compared to other functional groups, and is not expected to be effective in functionalizing CPP. Consequently, the properties and functions of methyl-substituted CPPs have not been considered in CPP chemistry. Even with such a simple methyl group, we envisioned that multiple substitutions on CPP may endow it with unique properties. In addition, the unique reactivity at the benzyl position allows further conversion and may be a key intermediate in the synthesis of new CPP derivatives and nanobelts.

Herein, we report the synthesis and properties of dodecamethyl[6]CPP (Me_{12}[6]CPP, **1**), composed of *o*-xylene units. The phenylene moieties of Me_{12}[6]CPP cannot rotate at room temperature because of the steric hindrance of the methyl groups, resulting in the isolation of two isomers (rotamers): **1-out** (D_{3d} symmetry), with all methyl groups facing outward, and **1-in** (C_s symmetry), with two methyl groups on one *o*-xylene unit facing inward. Interestingly, fluorescence was observed for both isomers, even though pristine [6]CPP does not fluoresce.[18] Experimental and theoretical investigations revealed that the internal conversion that prevents fluorescence of [6]CPP is suppressed in **1** due to its high rotational barrier, leading to enhanced fluorescence. This simple yet pronounced "methyl effect" in CPPs should contribute not only to the basic understanding of stereoelectronic effects in CPPs, but also to the design and application of CPP-based materials in various fields.

The synthesis of **1** was achieved using the gold-based method reported by Tsuchido, Osakada, *et al.* in 2020 (Fig. 2A).[4] Thus, (2,2′,3,3′-tetramethyl-[1,1′-biphenyl]-4,4′-diyl) diboronic acid bispinacol ester (**2**) and $[Au_2Cl_2(dcpm)]$ were reacted in the presence of Cs_2CO_3 at 50 °C in toluene/EtOH/H_2O to afford the corresponding macrocyclic gold complex. Then, $PhICl_2$ was applied to the macrocyclic gold complex at −60 °C in DMF and the resulting mixture was stirred at room temperature for 24 h to induce the aryl–aryl reductive elimination of the gold complex. After purification by column chromatography in chloroform, suspension in dichloromethane, and filtration, the target product **1-out** was isolated in 43% yield. The filtrate was

[a]*Department of Chemistry, Graduate School of Science, Nagoya University, Chikusa, Nagoya 464-8602, Japan. E-mail: yagi.akiko.r4@f.mail.nagoya-u.ac.jp*

[b]*Institute of Transformative Bio-Molecules (WPI-ITbM), Nagoya University, Nagoya 464-8602, Japan*

[c]*Molecule Creation Laboratory, Pioneering Research Institute, RIKEN, Wako, Saitama 351-0198, Japan. E-mail: kenichiro.itami@riken.jp*

[d]*Center for Sustainable Resource Science, RIKEN, Wako, Saitama, 351-0198, Japan*

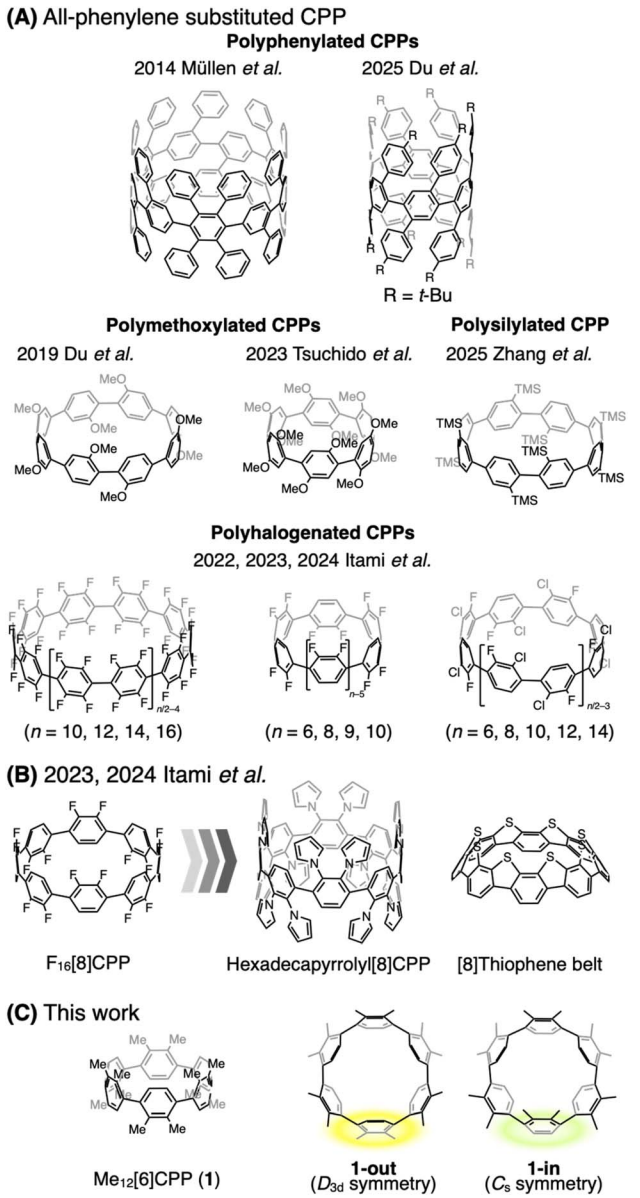

Fig. 1 (A) Examples of all-phenylene substituted CPPs. (B) Examples of the conversion of CPP into nanorings or nanobelts. (C) The structures of Me_{12}[6]CPP (**1**) and isomers (this work).

then subjected to gel permeation chromatography (GPC) to obtain the unexpected isomer **1-in** in 10% yield.

The structural feature of **1-out**, where all methyl groups face outside of the ring, was confirmed by X-ray crystallography, whereas the quality of crystals is not sufficient to be discussed (Fig. S3 and Table S2). In contrast, the crystal structure of the unexpected product **1-in** was successfully determined by X-ray crystallography, which revealed an inward-facing methyl group in one *o*-xylene unit, as shown in Fig. 2B. In the crystal structure, almost no solvent was identified in the internal cavity of CPP, which is considered to have voids. Noncovalent interaction (NCI) plots showed that the inward-facing methyl group is repulsed by a steric hindrance and stabilized by C–H$\cdots\pi$ interactions with the neighboring aromatic ring, and it also interacts with the hydrogen atom of the second neighboring aromatic ring (Fig. S9). The methyl effect was also identified in the packing structure. **1-in** adopts γ-type packing, whereas the pristine CPP series reported to date all show herringbone or tubular packing. The CPP ring voids are aligned in one dimension because of the obliquely aligned tubular structure of the CPP rings. Strong C–H$\cdots\pi$ interactions and dispersion forces in many directions were observed from the NCI plots (Fig. S10 and S11), indicating that the methyl groups have a significant effect on the molecular arrangement.

The ^{1}H NMR spectra of the **1-out** and **1-in** isomers differed significantly due to the different symmetries and the shielding effect from the neighboring aromatic ring. Due to the highly symmetric D_{3d} structure of **1-out**, two singlet signals at 6.22 ppm and 2.54 ppm were observed in the ^{1}H NMR spectrum corresponding to the aromatic and methyl groups, respectively. Notably, the aromatic signal was observed at a much higher magnetic field than that of pristine [6]CPP (7.64 ppm). This is because the hydrogen atoms of the aromatic rings in **1-out** experience an increased shielding effect from the neighboring aromatic rings due to the large dihedral angle (**1-out**: 45.1°, [6]CPP: 29.4°) caused by the methyl group places them inside the CPP ring. Significantly, this means that the rotation of the *o*-xylene unit is suppressed at room temperature. For comparison, the ^{1}H NMR spectrum of **1-in** is shown in Fig. 2C. This compound has C_s symmetry with a single symmetry plane. The *o*-xylene unit with the methyl groups facing inward experiences a very different shielding effect from the neighboring aromatic ring; consequently, the aromatic hydrogen atoms on the outside of the CPP ring (orange) are significantly shifted toward the lower-field side. Conversely, the benzylic hydrogen atoms (sky-blue) inside the CPP ring are shifted upfield. The ^{1}H signals assigned to the hydrogen atoms on the *o*-xylene unit on the opposite side of the CPP ring (green) are also observed as a singlet.

With this unexpected isomer pair in hand, we became interested in the isomerization process between **1-in** and **1-out**. First, the thermal stabilities of **1-in** and **1-out** were calculated using density functional theory (DFT) at the B3LYP-D3/6-31G(d) level of theory (Fig. 3A and B). The structural optimization results show that **1-in** is a semi-stable structure with 9.2 kcal mol^{-1} higher energy than **1-out**. Temperature-variable NMR (VT-NMR) measurements of **1-in** in 1,1,2,2-tetrachloroethane-d_2 (Fig. S4) revealed that isomerization of **1-in** to **1-out** occurred as the temperature increased. We then investigated the rotational barrier to this **1-in** to **1-out** isomerization by both DFT calculations and experiments. Although the rotation of the *o*-xylene unit can occur in two directions, the pathway in which the methyl groups are brought into close proximity was not considered because the steric hindrance would be too large. Calculations at the B3LYP-D3/6-31G(d) level revealed a transition state (TS) with a rotational barrier of 33.4 kcal mol^{-1}.

Based on the results obtained for the **1-in**-to-**1-out** isomerization, we determined the rotational barrier under mild heating conditions (Fig. 3C and D).[19] Thus, we monitored the rate of decrease in the **1-in** integral in the ^{1}H NMR spectra recorded in 1,1,2,2-tetrachloroethane-d_2 at several temperatures, with

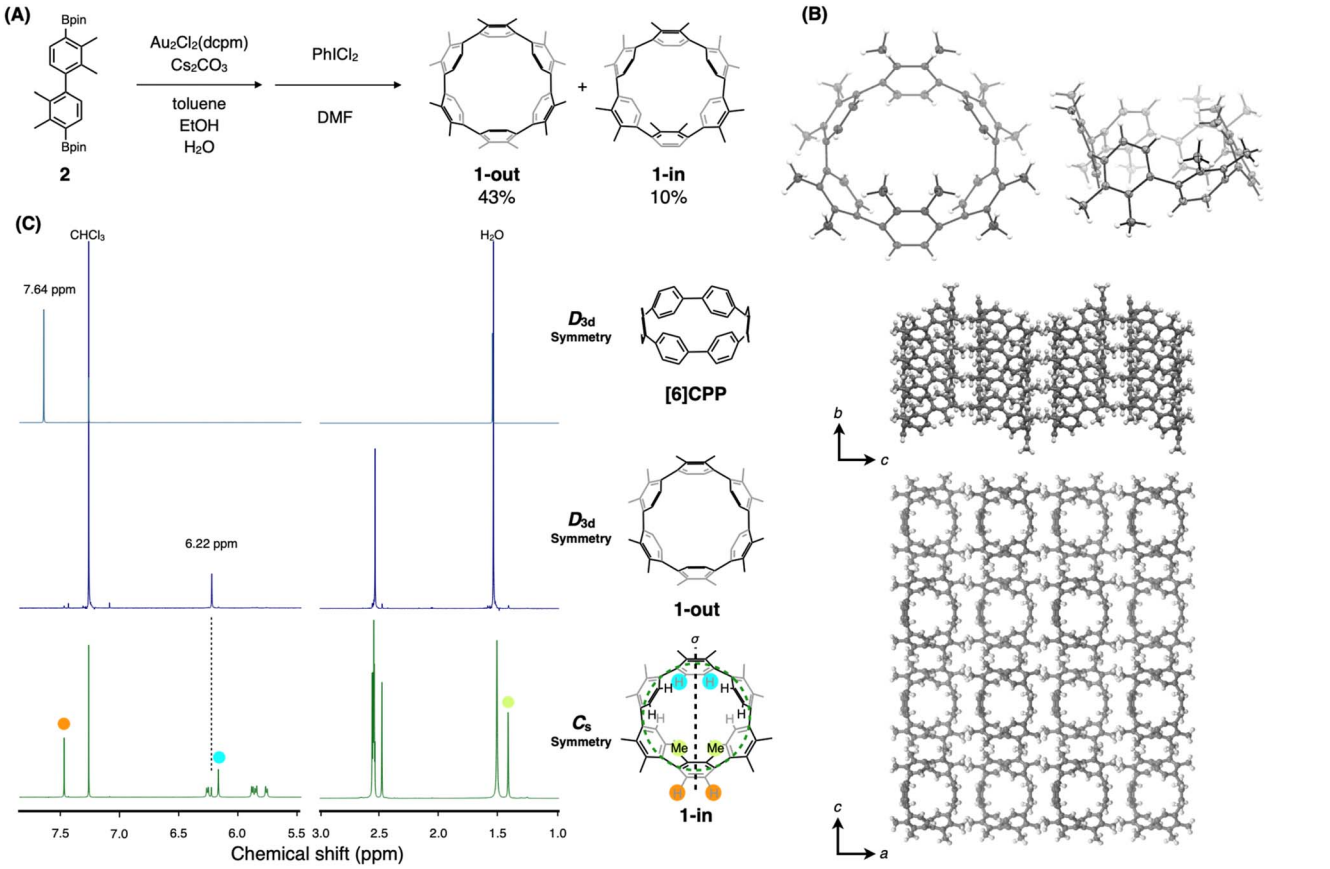

Fig. 2 (A) Synthesis of **1**. Reaction conditions: (i) **2** (1.0 equiv.), Au_2Cl_2(dcpm) (1.0 equiv.), Cs_2CO_3 (6.0 equiv.), toluene/EtOH/H_2O = 4 : 1 : 1, 50 °C, 24 h. (ii) Mixture product of (i), $PhICl_2$ (3.0 equiv.), DMF, −60 °C, 2 h, then, rt., 24 h. dcpm = bis(dicyclohexylphosphino)methane (B) ORTEP and packing structures of **1-in** with thermal ellipsoids at 50% probability. (C) ^{1}H NMR spectra of [6]CPP, **1-out**, and **1-in** (top to bottom, 600 MHz, $CDCl_3$). Green dash circle on **1-in** shows the CPP ring. Highlighted H and Me correspond to signals on the NMR spectrum.

coronene as an internal standard. The first-order rate constant for the isomerization at each temperature was determined. From an Eyring plot based on the obtained rate constants, the activation parameters were estimated to be $\Delta H^{\ddagger}$ = 29.5 kcal mol^{-1}, $\Delta S^{\ddagger}$ = 4.1 cal mol^{-1} K^{-1}, and $\Delta G^{\ddagger}_{298\ K}$ = 28.3 kcal mol^{-1}.

For comparison, the rotational barrier for the phenylene unit of [6]CPP was estimated by DFT calculations under similar conditions. Two transition states and one intermediate were found in the rotational path of [6]CPP. The largest TS (TS2) is 16.9 kcal mol^{-1} with a dihedral angle close to 90°. Noting that the TS1 of **1** has the structure with dihedral angle close to 0°, this corresponds to the structure of TS3 in [6]CPP. The steric hindrance of the methyl group possibly enhances the energy of this transition state, and as a result, the isomer of **1-in** could be isolated.

The high rotational barrier of **1** is the key to obtaining isolable isomers. Following this surprising discovery, we wondered how many methyl groups are required to generate a rotational barrier that is sufficient to allow isomers to be isolated. To address this question, we performed DFT calculations to estimate the rotational barrier for the isomerization of the in- to the out-isomer with different numbers of methyl groups (Fig. 4 and S13). In the case of Me_1[6]CPP (**3**), isomerization occurs *via* a simple pathway. The rotational barrier is 4.4 kcal mol^{-1}, which is comparable to that of TS3 of [6]CPP, suggesting that isomerization occurs easily at room temperature. We then considered systems with two methyl groups (Me_2[6]CPP, **4** and **5**). In the case of **4**, with two methyl groups on a single phenylene unit, the rotational barrier is 2.6 kcal mol^{-1}, despite the increased steric hindrance, which is attributed to the higher energy of the in-isomer compared to that of the out-isomer. In the case of **5**, which has two adjacent phenylene units bearing one methyl group each, two TSs and one intermediate were found when the methyl groups were rotated to avoid collisions between them. The energy difference between the in- and out-isomers is approximately the same as that of **3**, and the energy difference when one methyl group faces inward is approximately the same. The two TSs have similar energies and are comparable to the TS (out to in) of **4**; therefore, a rotational barrier of 13–14 kcal mol^{-1} is expected when two Ar–H/CH_3 groups are involved.

For Me_4[6]CPP (**6**), two TSs and one intermediate were identified. The maximum rotational barrier for isomerization from the in- to out-isomer is 13.0 kcal mol^{-1} and the four Ar–H/CH_3 groups look sterically hindered; therefore the isomerization is expected to occur easily at room temperature. However, for the first time, the energy of the TS associated with the

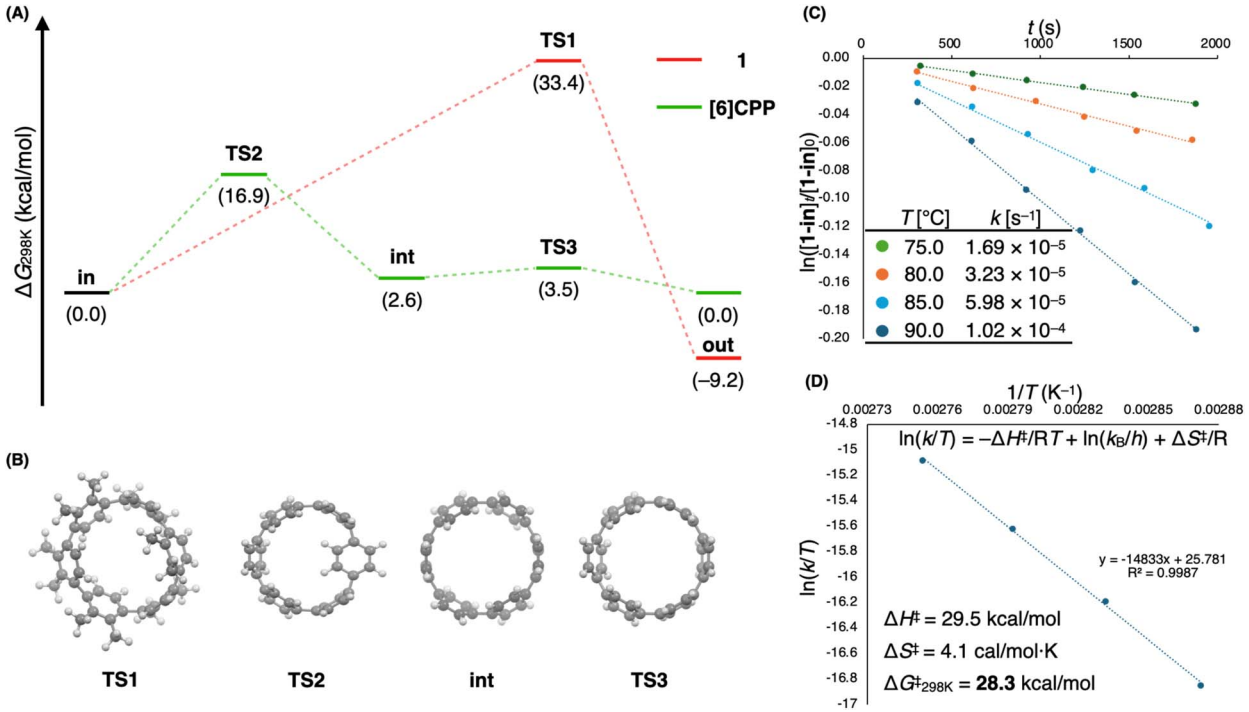

Fig. 3 (A) Transition states for *o*-xylenylene or phenylene unit rotation of **1** and [6]CPP. (B) Structures of TS1, TS2, TS3, and int (intermediate). These results was calculated at B3LYP-D3/6-31G(d) level of theory. (C) Plots for the decreasing integration of **1-in** in the ^{1}H NMR spectra upon heating at 75.0, 80.0, 85.0 and 90.0 °C in 1,1,2,2-tetrachloroethane-d_2, using coronene as the internal standard. (D) Eyring plot of thermal isomerization of **1-in** to **1-out**.

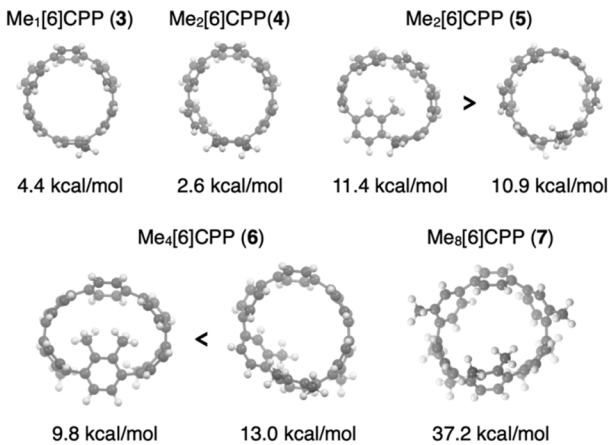

Fig. 4 Transition state energy for isomerization of Me$_n$[6]CPP (from in to out) calculated at B3LYP-D3/6-31G(d) level of theory.

inversion from the out-isomer exceeded the rotational barrier of [6]CPP. Upon further increasing the number of methyl groups, in Me$_8$[6]CPP (**7**), only one TS was found, with a very high rotational barrier of 37.2 kcal mol^{-1}. Because this rotational barrier prevents rotation at room temperature, it was concluded that eight or more adjacent methyl groups are required to obtain isolable isomers.

We found that the pronounced "methyl effect" in CPP is also manifested in the molecular orbitals and photophysical properties (Fig. 5). For example, the maximum absorption wavelengths of **1-out** and **1-in** (as solutions in toluene) were observed at 304 and 291 nm, respectively (Fig. 5A). The absorption corresponding to the HOMO–LUMO transition was observed as a shoulder peak. The shorter maximum absorption wavelength of **1-in** stems from its larger dihedral angle. DFT and TD-DFT calculations revealed that the HOMO–LUMO energy gap of **1-in** is larger than that of **1-out** (Fig. 5B). These absorption wavelengths are shorter than those of [6]CPP (339 nm), and the HOMO–LUMO energy gap is larger than that of [6]CPP. This is because the quinoidal LUMO is greatly destabilized by the larger dihedral angle owing to the steric hindrance imposed by the methyl group.

In contrast, the HOMO energy of **1-out** is slightly higher than that of [6]CPP, and **1-in** has a slightly lower HOMO energy than [6]CPP. Because methyl groups tend to be electron-donating, their introduction is expected to increase the HOMO and LUMO energies. DFT calculations revealed a change in the orbital energy depending on the number of methyl groups (Fig. 5C). The LUMO energy increased as the number of methyl groups increased. In contrast, the HOMO energy increased up to the 12th methyl group, and the introduction of additional methyl groups resulted in a decrease in the HOMO energy. Me$_{12}$[6]CPP was calculated to have the highest HOMO energy among the methylated CPP family. The shift in HOMO energy can be discussed in terms of the dihedral angles between the phenylene groups. The average dihedral angles of compounds with 1–6, 6–12, and 12–18 methyl groups show different shifts; in particular, the introduction of 12–18 methyl groups changes

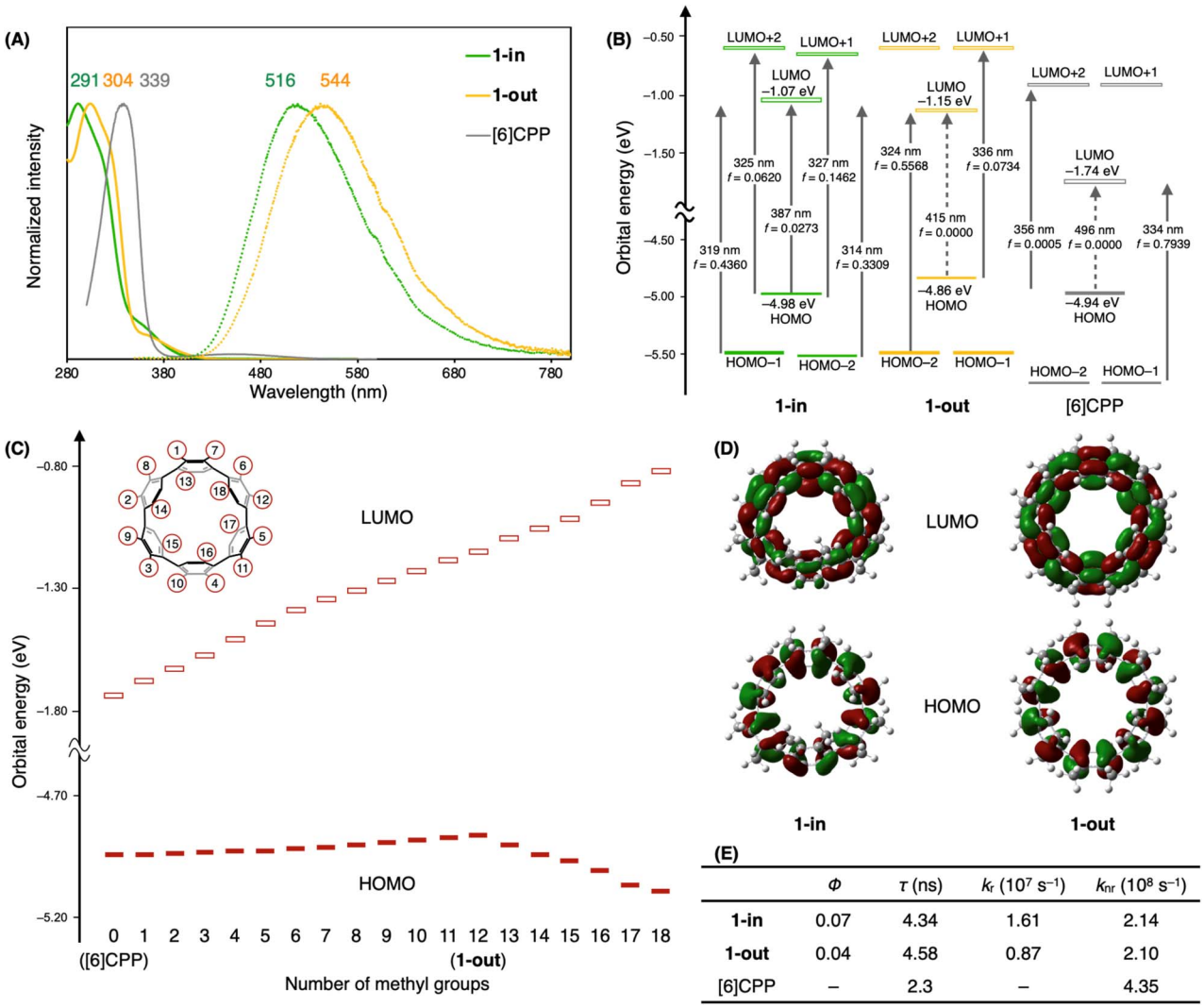

(E)

	Φ	τ (ns)	k_r (10^7 s^{-1})	k_{nr} (10^8 s^{-1})
1-in	0.07	4.34	1.61	2.14
1-out	0.04	4.58	0.87	2.10
[6]CPP	–	2.3	–	4.35

Fig. 5 (A) UV-Vis absorption spectra and fluorescence spectra of **1-in**, **1-out**, and [6]CPP in toluene solution. (B) TD-DFT calculations of **1-in**, **1-out**, and [6]CPP were calculated at the B3LYP/6-31+G(d,p) level of theory. Orbital energies were obtained at the B3LYP-D3/6-31G(d) level of theory. (C) Dependence of the orbital energies on the number of methyl groups calculated at B3LYP-D3/6-31G(d) level of theory. (D) Frontier molecular orbitals (isovalue: 0.02) were obtained at the B3LYP-D3/6-31G(d) level of theory. (E) Fluorescence quantum yield (Φ), lifetime (τ), radiative (k_r) and nonradiative (k_{nr}) rate constant of **1-in**, **1-out**, and [6]CPP.

the dihedral angles significantly. It is likely that, in these cases, the dihedral angle and the electron-donating nature of the methyl group are no longer balanced, which results in a decrease in the HOMO energy. These orbital energies are also discussed in terms of the bent angle. However, in this series, even when the number of methyl groups increases, there is no significant change in the bent angle, and the contribution of the bent angle on orbital energy is very small. Therefore, the dihedral angle and the electron-donating character of the methyl group dominate the change in orbital energy. The calculations for the structure with methyl group substituted at the *para*-position also showed that the dihedral angle is larger (51.7°) than that of the *ortho*-substituted structure, resulting in a lower HOMO energy (Fig. S15). The lower HOMO energy of **1-in** can also be attributed to its larger dihedral angle.

The fluorescence spectra were measured at an excitation wavelength of 300 nm. Surprisingly, Me_{12}[6]CPP showed fluorescence emission at approximately 510 nm for **1-in** and 540 nm for **1-out**. This is in sharp contrast to pristine [6]CPP, which is nonfluorescent; thus, a simple methyl substitution induces fluorescence from a nonfluorescent π-system. To confirm that these emissions were derived from Me_{12}[6]CPP, the fluorescence wavelength was set to 540 nm and the excitation spectrum was measured (Fig. S8). Under these conditions, the obtained excitation spectra were similar to the absorption spectra, indicating the fluorescence was derived from **1-in** and **1-out**. The fluorescence quantum yields were calculated to be 0.07 for **1-in** and 0.04 for **1-out**; the higher fluorescence quantum yield for **1-in** is likely due to the reduced symmetry (Fig. 5D). [6]CPP is nonfluorescent, which has been attributed to rapid deactivation through internal conversion.[20] On/off fluorescence was revealed by determining the rate constant of the nonradiative deactivation process (k_{nr}) (Fig. 5E). Based on the reported lifetime of the S_1 state of [6]CPP measured in THF,[20]

the k_{nr} value of [6]CPP was determined to be 4.35×10^8 s^{-1}. On the other hand, the k_{nr} value of Me_{12}[6]CPP was determined to be 2.1×10^8 s^{-1} based on the fluorescence lifetime and quantum yield. The k_{nr} value of Me_{12}[6]CPP was approximately two times lower than that of [6]CPP. Thus, it is likely that the high rotational barrier of Me_{12}[6]CPP suppresses the non-radiative deactivation process through internal conversion, which may explain its fluorescence.

Another report concluded that the dihedral angle affects the excited state and that the electron–hole distribution becomes more localized as the dihedral angle increases.[21] Therefore, the structure optimization and TD-DFT calculations for the S_1 state were performed. The calculations at the CAM-B3LYP-D3/6-31G(d,p) level indicate that even the highly symmetric out-isomer has a small but non-zero oscillator strength and may contribute to the emission process (Fig. S15, S16 and Table S7). However, structural flattening in the S_1 state has not been confirmed in Me_{12}[6]CPP, as observed in the fluorescence mechanism of CPP with a large dihedral angle. This suggests that, in Me_{12}[6]CPP, the suppression of vibrational deactivation due to steric hindrance is a key factor influencing its fluorescence.

Conclusions

In summary, we have synthesized dodecamethyl[6]CPP, a [6]CPP composed of *o*-xylene units, and investigated its physical properties. The introduction of a large number of methyl groups into the backbone has unique effects on the CPPs due to the steric bulk of the methyl groups. Dodecamethyl[6]CPP adopted two isomers, **1-in** and **1-out**, owing to the suppression of aromatic ring rotation at room temperature. The structure of **1-in** was determined by X-ray crystallography and showed an unusual packing structure due to multidirectional interactions. Its high rotational barrier enables fluorescence by preventing the internal conversion that suppresses the fluorescence of [6]CPP. This simple yet significant "methyl effect" in CPPs helps clarify the fundamental stereoelectronic effects that act on CPPs, and should facilitate the design and application of CPP-based materials in various fields.

Author contributions

A. Y. and K. I. conceived the concept and directed the project. T. K. performed synthesis, all experimental measurements and DFT calculations. D. I. performed and analyzed X-ray crystallography. T. K., A. Y., and K. I. wrote the manuscript with feedback from D. I. All authors approved the final version of the manuscript.

Conflicts of interest

There are no conflicts to declare.

Data availability

CCDC 2414709 contains the supplementary crystallographic data for this paper.[22]

The data that support the findings of this study are available in the SI of this article. See DOI: https://doi.org/10.1039/d5sc04694g.

Acknowledgements

This work is supported by JSPS KAKENHI grants (19H05463 to K. I., 25H00429 to K. I., 22K21346 to A. Y., 25H01255 to A. Y.). T. K. and D. I. thank the JSPS fellowship for young scientists and Nagoya University Graduate Program of Transformative Chem-Bio Research (WISE program) supported by MEXT. The computations were performed using the Research Center for Computational Science, Okazaki, Japan (Project No. 23-IMS-C123, 24-IMS-C117, 25-IMS-C119). The authors thank Dr Kinichi Oyama and Ms Rio Yamada (RCMS, Nagoya University) for their support in the NMR study.

Notes and references

1 R. Jasti, J. Bhattacharjee, J. B. Neaton and C. R. Bertozzi, *J. Am. Chem. Soc.*, 2008, **130**, 17646–17647.
2 H. Takaba, H. Omachi, Y. Yamamoto, J. Bouffard and K. Itami, *Angew. Chem., Int. Ed.*, 2009, **48**, 6112–6116.
3 S. Yamago, Y. Watanabe and T. Iwamoto, *Angew. Chem., Int. Ed.*, 2010, **49**, 757–759.
4 Au-based method: Y. Tsuchido, R. Abe, T. Ide and K. Osakada, *Angew. Chem., Int. Ed.*, 2020, **59**, 22928–22932.
5 Ni-based method: H. Shudo, M. Kuwayama, M. Shimasaki, T. Nishihara, Y. Takeda, N. Mitoma, T. Kuwabara, A. Yagi, Y. Segawa and K. Itami, *Nat. Commun.*, 2022, **13**, 3713.
6 Reviews: (*a*) E. R. Darzi and R. Jasti, *Chem. Soc. Rev.*, 2015, **44**, 6401–6410; (*b*) Y. Segawa, A. Yagi, K. Matsui and K. Itami, *Angew. Chem., Int. Ed.*, 2016, **55**, 5136–5158; (*c*) S. E. Lewis, *Chem. Soc. Rev.*, 2015, **44**, 2221–2304; (*d*) Y. Li, H. Kono, T. Maekawa, Y. Segawa, A. Yagi and K. Itami, *Acc. Mater. Res.*, 2021, **2**, 681–691; (*e*) E. J. Leonhardt and R. Jasti, *Nat. Rev. Chem.*, 2019, **3**, 672–686; (*f*) M. Hermann, D. Wassy and B. Esser, *Angew. Chem., Int. Ed.*, 2021, **60**, 15743–15766; (*g*) R. Roy, C. Brouillac, E. Jacques, C. Quinton and C. Poriel, *Angew. Chem., Int. Ed.*, 2024, **63**, e202402608.
7 (*a*) T. Iwamoto, Y. Watanabe, T. Sadahiro, T. Haino and S. Yamago, *Angew. Chem., Int. Ed.*, 2011, **50**, 8342–8344; (*b*) A. V. Zabula, A. S. Filatov, J. Xia, R. Jasti and M. A. Petrukhina, *Angew. Chem., Int. Ed.*, 2013, **55**, 5033–5036; (*c*) E. Kayahara, T. Kouyama, T. Kato, H. Takaya, N. Yasuda and S. Yamago, *Angew. Chem., Int. Ed.*, 2013, **52**, 13722–13726; (*d*) Y. Nakanishi, H. Omachi, S. Matsuura, Y. Miyata, R. Kitaura, Y. Segawa, K. Itami and H. Shinohara, *Angew. Chem., Int. Ed.*, 2014, **53**, 3102–3106; (*e*) N. Toriumi, A. Muranaka, E. Kayahara, S. Yamago and M. Uchiyama, *J. Am. Chem. Soc.*, 2015, **21**, 82–85; (*f*) E. Kayahara, T. Kouyama, T. Kato and S. Yamago, *J. Am. Chem. Soc.*, 2016, **138**, 338–344; (*g*) H. Ueno, T. Nishihara, Y. Segawa and K. Itami, *Angew. Chem., Int. Ed.*, 2015, **54**, 3707–3711; (*h*) H. Sakamoto, T. Fujimori, X. Li, K. Kaneko, K. Kan, N. Ozaki, Y. Hijikata, S. Irle and K. Itami, *Chem. Sci.*, 2016, **7**, 4204–4210; (*i*) N. Ozaki, H. Sakamoto,

T. Nishihara, T. Fujimori, Y. Hijikata, R. Kimura, S. Irle and K. Itami, *Angew. Chem., Int. Ed.*, 2017, **56**, 11196–11202; (*j*) E. Kayahara, L. Sun, H. Onishi, K. Suzuki, T. Fukushima, A. Sawada, H. Kaji and S. Yamago, *J. Am. Chem. Soc.*, 2017, **139**, 18480–18483; (*k*) N. S. Spisak, Z. Wei, E. Darzi, R. Jasti and M. A. Petrukhina, *Chem. Commun.*, 2018, **54**, 7818–7821; (*l*) E. J. Leonhardt, J. M. Van Raden, D. J. Miller, L. N. Zakharov, B. J. Alemán and R. Jasti, *Nano Lett.*, 2018, **18**, 7991–7997; (*m*) R. L. Maust, P. Li, B. Shao, S. M. Zeitler, P. B. Sun, H. W. Reid, L. N. Zakharov, M. R. Golder and R. Jasti, *ACS Cent. Sci.*, 2021, **7**, 1056–1065; (*n*) Y. Lv, J. Lin, K. Song, X. Song, H. Zang, Y. Zang and D. Zhu, *Sci. Adv.*, 2021, **7**, eabk3095; (*o*) P. Hall, H. Reid, I. Liashenko, B. Tandon, K. O'Neill, G. Lindberg, R. Jasti and P. Dalton, *Small*, 2024, **20**, 2400882; (*p*) D. Imoto, H. Shudo, A. Yagi and K. Itami, *Angew. Chem., Int. Ed.*, 2024, **63**, e202413828.

8 (*a*) B. M. White, Y. Zhao, T. E. Kawashima, B. P. Branchaud, M. D. Pluth and R. Jasti, *ACS Cent. Sci.*, 2018, **4**, 1173–1178; (*b*) T. C. Lovell, S. G. Bolton, J. P. Kenison, J. Shangguan, C. E. Otteson, F. Cevitci, X. Nan, M. D. Pluth and R. Jasti, *ACS Nano*, 2021, **15**, 15285–15293; (*c*) K. Günther, H. Kono, H. Shudo, D. Shimizu, R. Isoda, M. Nakamura, A. Yagi, K. Amaike and K. Itami, *Angew. Chem., Int. Ed.*, 2024, **63**, e202414645.

9 (*a*) Y. Segawa, M. Kuwayama, Y. Hijikata, M. Fushimi, T. Nishihara, J. Pirillo, J. Shirasaki, N. Kubota and K. Itami, *Science*, 2019, **365**, 272–276; (*b*) Y. Li, Y. Segawa, A. Yagi and K. Itami, *J. Am. Chem. Soc.*, 2020, **142**, 12850–12856; (*c*) H. Kono, Y. Li, R. Zanasi, G. Monaco, F. F. Summa, L. T. Scott, A. Yagi and K. Itami, *J. Am. Chem. Soc.*, 2023, **145**, 8939–8946.

10 (*a*) Y. Segawa, H. Ito and K. Itami, *Nat. Rev. Mater.*, 2016, **1**, 15002; (*b*) I. A. Stepek, M. Nagase, A. Yagi and K. Itami, *Tetrahedron*, 2022, **123**, 132907.

11 F. E. Golling, M. Quernheim, M. Wagner, T. Nishiuchi and K. Müllen, *Angew. Chem., Int. Ed.*, 2014, **53**, 1525–1528.

12 W. Zhang, J. Wang, X. Zhang, B. Yuan, P. Fang, N. Yin and P. Du, *Angew. Chem., Int. Ed.*, 2025, **64**, e202508017.

13 S. Cui, G. Zhuang, J. Wang, Q. Huang, S. Wang and P. Du, *Org. Chem. Front.*, 2019, **6**, 1885–1890.

14 N. Narita, Y. Kurita, K. Osakada, T. Ide, H. Kawai and Y. Tsuchido, *Nat. Commun.*, 2023, **14**, 8091.

15 Y. Ren, W. Shang, H. Sun, Q. Liang, E. Kayahara, S. Yamago, Y. Li and D. Zhang, *J. Org. Chem.*, 2025, **90**, 8959.

16 (*a*) Ref. 5;; (*b*) H. Shudo, M. Kuwayama, Y. Segawa, A. Yagi and K. Itami, *Chem. Commun.*, 2023, **59**, 13494–13497; (*c*) D. Imoto, H. Shudo, K. Mizukami, N. Kimizuka, A. Yagi and K. Itami, *Chem. Commun.*, 2024, **60**, 12585–12588; (*d*) H. Shudo, P. Wiesener, E. Kolodzeiski, K. Mizukami, D. Imoto, H. Mönig, S. Amirjalayer, H. Sakamoto, H. Klaasen, B. J. Ravoo, N. Kimizuka, A. Yagi and K. Itami, *Nat. Commun.*, 2025, **16**, 1074.

17 D. Imoto, A. Yagi and K. Itami, *Precis. Chem.*, 2023, **1**, 516–523.

18 (*a*) J. Xia and R. Jasti, *Angew. Chem., Int. Ed.*, 2012, **51**, 2474–2476; (*b*) E. Kayahara, T. Iwamoto, T. Suzuki and S. Yamago, *Chem. Lett.*, 2013, **42**, 621–623; (*c*) E. Kayahara, V. K. Patel, J. Xia, R. Jasti and S. Yamago, *Synlett*, 2015, **26**, 1615–1619; (*d*) T. Fukushima, H. Sakamoto, K. Tanaka, Y. Hijikata, S. Irle and K. Itami, *Chem. Lett.*, 2017, **46**, 855–857.

19 K. Okada, A. Yagi, Y. Segawa and K. Itami, *Chem. Sci.*, 2017, **8**, 661–667.

20 M. Fujitsuka, C. Lu, B. Zhuang, E. Kayahara, S. Yamago and T. Majima, *J. Phys. Chem. A*, 2019, **123**, 4737–4742.

21 S. Chen, X. Miao, H. Zhou, C. Peng, R. Zhang and X. Han, *J. Phys. Chem. A*, 2022, **126**, 7452–7459.

22 T. Kato, D. Imoto, A. Yagi and K. Itami, CCDC 2414709: Experimental Crystal Structure Determination, 2025, DOI: **10.5517/ccdc.csd.cc2m1pv7**.